scientific reports

Check for updates

OPEN

Effective mathematical modelling of health passes during a pandemic

Stefan Hohenegger[1,2], Giacomo Cacciapaglia[1,2]✉ & Francesco Sannino[3,4,5]

We study the impact on the epidemiological dynamics of a class of restrictive measures that are aimed at reducing the number of contacts of individuals who have a higher risk of being infected with a transmittable disease. Such measures are currently either implemented or at least discussed in numerous countries worldwide to ward off a potential new wave of COVID-19. They come in the form of Health Passes (HP), which grant full access to public life only to individuals with a certificate that proves that they have either been fully vaccinated, have recovered from a previous infection or have recently tested negative to SARS-Cov-2. We develop both a compartmental model as well as an epidemic Renormalisation Group approach, which is capable of describing the dynamics over a longer period of time, notably an entire epidemiological wave. Introducing different versions of HPs in this model, we are capable of providing quantitative estimates on the effectiveness of the underlying measures as a function of the fraction of the population that is vaccinated and the vaccination rate. We apply our models to the latest COVID-19 wave in several European countries, notably Germany and Austria, which validate our theoretical findings.

The epidemiological dynamics of SARS-Cov-2 in many countries has been characterised by several waves. These are periods of exponential growth in the number of infected individuals, followed by (quasi-)linear growth phases. Modelling this dynamics in 2021 is involved due to a number of different factors: (1) the availability of several different vaccines, which started being deployed at the end of 2020, and national vaccination campaigns around the globe; (2) the appearance of several variants of SARS-Cov-2 , which differ in their infection rate[1–4] and their ability to avoid antibody responses (recent theoretical[5] and numerical[6] studies explore the impact of variants on the pandemic diffusion); (3) non-pharmaceutical interventions (ranging from lockdowns to various degrees of social distancing measures) taking into account economical, social and political factors. In particular regarding i), roughly 37% of the global population is fully vaccinated as of the end of October 2021, see Ourworldindata.org, however with only very few countries having reached a rate of $>$ 50%, which is still largely below the projected herd-immunity threshold.

With the number of vaccinated adult individuals rising (but still staying below the herd immunity threshold, in particular for the more aggressive new Delta-variant) and in an attempt to further allow social life to return to levels similar to the ones before the pandemic, many countries have discussed (and in several cases also adopted) social distancing measures that are tailored according to the threat an individual poses to infect others. Such measures require individuals to present certificates, which prove that they present a low risk of being infectious, in order to participate in the public life. The certificates attest that the person is fully vaccinated against COVID-19 (after having received the required number of doses of an approved vaccine and a certain waiting time), or that they have recovered from a not too distant infection or that they have recently tested negative for SARS-Cov-2. In fact, different combinations of the above are present at national level. The social measure requires to present the certificate before entering locations or events where the risk of contagion is high[7], such as public places (restaurants, bars, museums, shopping malls etc.), social events (concerts, theatres, cinemas etc.), public means of transportation (trains, airplanes,etc.) or universities and schools. Since the specifics and the names differ from country to country, in the following we shall collectively refer to these certificates as *Health Passes* (HPs). Examples for concrete implementations in different European countries can be found in Section S6.1 of the Supplementary Material.

The objective of our work is to develop a simple and economical mathematical model that allows to analyse the impact of different versions of HPs on the epidemiological dynamics of an entire wave of a pandemic. The

[1]Institut de Physique des 2 Infinis (IP2I) de Lyon, CNRS/IN2P3, UMR5822, 69622 Villeurbanne, France. [2]Université de Lyon, Université Claude Bernard Lyon 1, 69001 Lyon, France. [3]Scuola Superiore Meridionale, Largo S. Marcellino, 10, 80138 Naples, NA, Italy. [4]Dipartimento di Fisica, E. Pancini, Università di Napoli, Federico II and INFN sezione di Napoli, Complesso Universitario di Monte S. Angelo Edificio 6, via Cintia, 80126 Naples, Italy. [5]CP3-Origins and D-IAS, University of Southern Denmark, Campusvej 55, 5230 Odense, Denmark. ✉email: g.cacciapaglia@ipnl.in2p3.fr

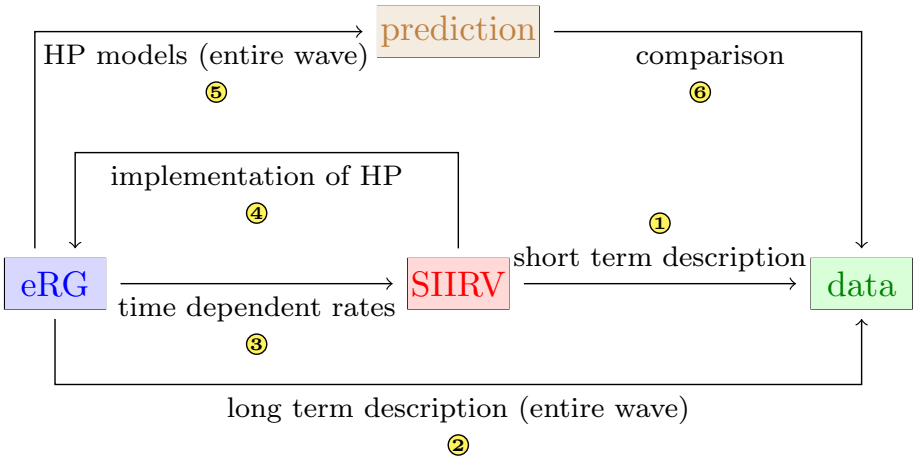

Figure 1. Schematic overview of the interplay between a compartmental model (SIIRV) and an eRG approach to arrive at quantitive prediction on HP measures from input data.

mathematical modelling of infectious diseases has a long standing history, and several different approaches exist in the literature: these range from stochastic methods[8–13] to deterministic compartmental models[14–16] (including the effect of vaccines[17–20]) to computer- and data driven approaches[21–25] and network models[26–28]. The advent of SARS-Cov-2 has caused a spike of research activity, with new models exploring key aspects of the pandemic, for example its multi-wave structure[29,30] and the evaluation of its impact on society and economy[31–36]. Models that quantify the impact of non-pharmaceutical interventions have also been proposed[37–40] and validated on the COVID-19 available data. Nevertheless, the specific impact of HPs has not been studied in the literature yet, and our work aims at covering this gap. In the current work we shall exploit the interplay between two types of models, namely a *compartmental model* and the *epidemiological Renormalisation Group* (eRG) approach. The former is among the oldest approaches[14] (see[16,41] for further references) and it treats the spread of an infectious disease by dividing the population into several compartments containing individuals in different states with respect to the disease (e.g. susceptible, exposed, infectious, recovered etc.). The passage of individuals from one compartment to another is described through a set of coupled first order differential equations in time, which can be seen as a continuous mean-field approximations of a more microscopic description of the infections[12,13,41]. Models of this type can be easily adapted and extended[31] by adding compartments[42,43], stratifying them in terms of age groups or geographical location[44] and upgrading the parameter to functions of time for a better fit to the data. Compartmental models are particularly useful in establishing qualitative relations between microscopic aspects of the spread of the disease among individuals and more macroscopic observables, such as the total number of individuals who have become infected at the end of an epidemic wave. However, in their simplest incarnation with constant transition rates, these models are capable of describing the time evolution accurately only over a relatively short period of time. Due to the fact that the epidemiological situation constantly changes (as we explained above), the rates need to be adapted as functions of time. The eRG framework has been introduced[29,30] to capture, more efficiently, the time evolution of the disease diffusion by explicitly taking into account symmetry, being inspired by the physical concepts of time-invariance symmetry and fixed points (the concept of Renormalisation Group Equations (RGE) has been originally developed in the context of statistical and particle physics[45–47]). Concretely, the eRG framework takes the form of a set of flow equations (called the β-functions) that describe the evolution of a quantity of epidemiological interest (e.g. a smooth monotonic function of the cumulative number of infected individuals I_c) as the flow between different fixed points. It has been demonstrated[48,49] that the eRG approach is indeed capable of describing accurately not only a full wave of COVID-19, but is also capable of modelling more complex multi-wave structures[50,51] even under changing conditions, like the appearance of new variants[5], vaccination dynamics[52], change in the social dynamics[53], among the ones mentioned above.

In this work we studied the effectiveness of HPs by combining the flexibility of compartmental models in capturing microscopic details of the spread of a disease and their relation to more macroscopic quantities within an eRG framework. The latter efficiently encapsulates the symmetries and long-term aspects of epidemics. The methodology we followed is schematically illustrated in Fig. 1: we first introduce a compartmental model (called SIIRV) which contains 5 compartments, namely S (unvaccinated susceptible), I_1 (unvaccinated infectious), I_2 (previously vaccinated infectious), R (removed) and V (vaccinated susceptible). Although vaccines have fairly high efficacies in preventing infections in the vaccinated population (around 80–90% for the best cases), here we take into account the fact that vaccines neither grant complete immunity against an infection from SARS-Cov-2 nor prevent the transmission of the virus from an infected vaccinated individuals to others. Assuming constant rates at which individuals pass between these compartments, this model is capable of fitting epidemiological data only over a short period of time ①. Alas, this class of models is not capable of describing correctly the dynamics of an entire wave of COVID-19. Hence, we ensure a correct description of the epidemiological data via the eRG framework ②. Matching the solutions of the SIIRV model with the eRG provides time-dependent infection and removal rates ③, which allow to extend the range of validity of the compartmental model to accurately reproduce the data. We then implement two different types of HP-models at the level of the SIIRV model (with

time-dependent rates): the net effect is a reduction in the contact rates between certain classes of individuals, thus corresponding to a systematic re-scaling of certain terms in the differential equations controlled by an efficacy parameter p. Studying the dynamics of the resulting system allows us to implement the HP-models in the eRG ④ by introducing a p-dependence in its parameters. This provides us with a model that not only allows to make long-term predictions ⑤ for HP-models but also to compare ⑥ different types of HP among each other and the current situation in different countries.

We consider two different types of HP-measures putting different emphasis on vaccinated versus unvaccinated individuals:

- Vaccine and Test Health Passes (VT-HP): individuals with a certificate of a negative test against SARS-Cov-2 are granted the same level of access to public life as people who have been vaccinated. We implicitly assume, in this scenario, that tests are easily accessible (and free of charge) for the majority of the population. Examples for models of this type which have actually been implemented are the Austrian '3-G-Regel', the Danish 'Corona Pass' or the French 'pass sanitaire' .
- Vaccine Health Passes (V-HP): only individuals who posses a certificate for being completely vaccinated against SARS-Cov-2 are granted unrestricted access to public life

In both cases, individuals that have previously contracted the disease are considered as fully immunised. Currently, there are several examples of VT-HPs implemented in various countries, while (to our knowledge) V-HPs are currently only being discussed. We consider the two HP models as templates of two extremal situations, and perform a comparative analysis of their effect on the long-term spread of the disease.

Methods

Compartmental vaccine model and health passes. We first introduce a compartmental model, conceived to describe and quantify the impact of HPs during a single epidemiological wave. For COVID-19, this requires a typical time-span of 1–2 months, hence variations in the population due to births, mobility and mortality play a minor role. Hence, the model we design is based on the following main assumptions:

1. A closed population, comprising of all the individuals that are susceptible of being infected during a single epidemic wave.
2. Negligible reinfection rates, hence all individuals that are unable to infect (deceased, recovered, quarantined, hospitalised individuals) are counted in a single compartment.
3. Merged categories when they are not distinguished by the application of the Health Pass: for simplicity, we do not consider deaths, hospitalisations, isolation, etc, as separate compartments. This greatly reduces the number of free parameters and improves on predictivity.
4. Separated compartments for vaccinated and un-vaccinated individuals.
5. Time-independent parameters (infection, recovery and vaccination rates).

This leads to the 5-compartment model, which we describe in detail below.

Basic SIIRV model. Our starting point is an isolated population of size $N \gg 1$, which we re-group into 5 basic compartments, as listed below.

- Susceptible: $N\,S(t)$ denotes the number individuals at time t who are not infectious and who have not been (fully) vaccinated. They can become infectious if they come in contact with the disease via an infectious individual.
- Vaccinated: $N\,V(t)$ denotes the number of individuals who, at time t, are not infectious and who are fully vaccinated. We shall, however, assume that these individuals can still get infected if they come in contact with the disease, but with a rate suppressed by a factor $\zeta < 1$ compared to S.
- Infectious: $N\,I_1(t)$ denotes the number of infectious individuals at time t who have not been previously vaccinated.
- Infectious: $N\,I_2(t)$ denotes the number of infectious individuals at time t who have been previously vaccinated.
- Removed: $N\,R(t)$ denotes the number of removed individuals at time t, who cannot become infectious. They account for previously infectious individuals who fully recovered, or are prevented from infecting due to some other removal mechanism (such as quarantine or death).

Individuals can pass from one of these compartments to another through various mechanisms, which we model through fixed rates $\gamma_{1,2}$ (infection), ε (removal) and ρ (vaccination rate). The processes are mathematically described by the following coupled first order differential equations in time:

$$\begin{aligned}
\frac{dS}{dt}(t) &= -S(t)\,[\rho + \gamma_1\,I_1(t) + \gamma_2\,I_2(t)], & \frac{dI_1}{dt}(t) &= S(t)\,[\gamma_1\,I_1(t) + \gamma_2\,I_2(t)] - \varepsilon\,I_1(t),\\
\frac{dV}{dt}(t) &= \rho\,S(t) - V(t)\,\zeta\,[\gamma_1\,I_1(t) + \gamma_2\,I_2(t)], & \frac{dI_2}{dt}(t) &= V(t)\,\zeta\,[\gamma_1\,I_1(t) + \gamma_2\,I_2(t)] - \varepsilon\,I_2(t), \qquad (1)\\
\frac{dR}{dt}(t) &= \varepsilon\,[I_1(t) + I_2(t)], &&
\end{aligned}$$

which need to be supplemented by the initial conditions

$$S(t=0)=S_0\,,\quad I_1(t=0)=I_{1,0}\,,I_2(t=0)=I_{2,0}\,,\quad V(t=0)=V_0\,,R(t=0)=0\,. \tag{2}$$

Here we assume the outbreak of the disease at $t=0$ and we normalise the initial conditions to satisfy $S_0+I_{1,0}+I_{2,0}+V_0=1$. In (1), $\gamma_1,\gamma_2\in\mathbb{R}_+$ are the rates at which infectious individuals with or without prior vaccination infect susceptible individuals. These two rates are not considered a priori the same (however, in most examples, for simplicity we used $\gamma_1=\gamma_2$). Furthermore, ε denotes the recovery rate, which is assumed to be independent of whether individuals have been previously vaccinated or not. We also define the ratios $\sigma_1=\frac{\gamma_1}{\varepsilon}$ and $\sigma_2=\frac{\gamma_2}{\varepsilon}$, which correspond to the reproduction numbers of the two infectious compartments. The rate ρ in (1) denotes the vaccination rate, which is chosen to be constant. Studying the examples of Germany and Austria, evidence is provided in Sections S6.2 and S6.3 of the Supplementary Material that this indeed leads to a reasonable approximation for a single wave of COVID-19. Finally, the efficacy of the vaccine is encoded in the reduction factor $\zeta\in[0,1)$ for the infection rate of vaccinated individuals, estimated from recent studies for different vaccines agains SARS-Cov-2[54]. For later use, we also define the cumulative number of infected individuals as a function of time:

$$I_{\mathrm{c}}(t)=N\,(I_{1,0}+I_{2,0})+N\int_0^t dt'\,\left[S(t')+\zeta\,V(t')\right]\,\left[\gamma_1\,I_1(t')+\gamma_2\,I_2(t')\right]. \tag{3}$$

Finally, the herd-immunity threshold for the vaccination dynamics encoded in eqs. (1) is $h^{\mathrm{HIT}}=\frac{\sigma_1-1}{\sigma_1-\zeta\sigma_2}$ (see Section S1.2 of the Supplementary Material for more details).

Implementing health passes. The factor ζ in the SIIRV model (1) mainly takes into account biological effects of the various vaccines and a priori is not related to any social distancing measures particularly targeted at unvaccinated individuals. HP-measures, instead, are specifically aimed at reducing social contacts of individuals posing a higher threat of infecting others by allowing access to public places and social events only to individuals who can either prove a certain level of immunisation against SARS-Cov-2 and/or have recently tested negative for the virus. To implement these measures into the SIIRV model, we distinguish the two conceptually different types of HPs, as described in the introduction:

- VT-HP: this model effectively only restricts the contacts of unvaccinated infectious individuals, i.e. those in the compartment I_1. In (1), we can implement such restrictions through a suppression factor $p_{\mathrm{VT}}\in[0,1]$ that takes into account how much contacts of the unvaccinated infectious individuals I_1 with the rest of the population are reduced

$$\begin{aligned}
\frac{dS}{dt}&=-S\left[\rho+p_{\mathrm{VT}}\,\gamma_1\,I_1(t)+\gamma_2\,I_2\right],\\
\frac{dI_1}{dt}&=S\left[p_{\mathrm{VT}}\,\gamma_1\,I_1+\gamma_2\,I_2\right]-\varepsilon\,I_1\,,\\
\frac{dV}{dt}&=\rho\,S-V\,\zeta\,\left[p_{\mathrm{VT}}\,\gamma_1\,I_1+\gamma_2\,I_2\right],\\
\frac{dI_2}{dt}&=V\,\zeta\,\left[p_{\mathrm{VT}}\,\gamma_1\,I_1+\gamma_2\,I_2\right]-\varepsilon\,I_2\,,\\
\frac{dR}{dt}&=\varepsilon\,[I_1+I_2]\,.
\end{aligned} \tag{4}$$

  Mathematically, the VT-HPcorresponds to a rescaling of the infection rate for unvaccinated individuals $\gamma_1\to p_{\mathrm{VT}}\gamma_1$. The cumulative number of infected individuals for this model becomes

$$I_{\mathrm{c}}^{(\mathrm{VT})}(t,p_{\mathrm{VT}})=N\,(I_{1,0}+I_{2,0})+N\int_0^t dt'\,\left[S(t')+\zeta\,V(t')\right]\,\left[p_{\mathrm{VT}}\,\gamma_1\,I_1(t')+\gamma_2\,I_2(t')\right]. \tag{5}$$

- V-HP: in models of this type, the social interactions of any unvaccinated individual (i.e. in the compartments S and I_1) are reduced. In (1), we can implement such restrictions through a suppression factor $p_{\mathrm{V}}\in[0,1]$ that measures the efficacy of this reduction

$$\begin{aligned}
\frac{dS}{dt}&=-S\left[\rho+p_{\mathrm{V}}^2\,\gamma_1\,I_1+p_{\mathrm{V}}\,\gamma_2\,I_2\right],\\
\frac{dI_1}{dt}&=S\left[p_{\mathrm{V}}^2\,\gamma_1\,I_1+p_{\mathrm{V}}\,\gamma_2\,I_2\right]-\varepsilon\,I_1\,,\\
\frac{dV}{dt}&=\rho\,S-V\,\zeta\,\left[p_{\mathrm{V}}\,\gamma_1\,I_1+\gamma_2\,I_2\right],\\
\frac{dI_2}{dt}&=V\,\zeta\,\left[p_{\mathrm{V}}\,\gamma_1\,I_1+\gamma_2\,I_2\right]-\varepsilon\,I_2\,,\\
\frac{dR}{dt}&=\varepsilon\,[I_1+I_2]\,.
\end{aligned} \tag{6}$$

The cumulative number of infected individuals is given by

$$I_{\rm c}^{(\rm V)}(t,p_{\rm V}) = N\,(I_{1,0}+I_{2,0}) + N\int_0^t dt'\,\left[p_{\rm V}\,S(t')+\zeta\,V(t')\right]\,\left[p_{\rm V}\,\gamma_1\,I_1(t')+\gamma_2\,I_2(t')\right]. \tag{7}$$

Epidemiological renormalisation group. Here we use the simplest eRG approach[29], which follows the time-evolution of the number of infections in a closed and isolated population over the time-span of a single wave. This formulation is enough to study the effect of HPs. In the literature, extensions of the eRG are available, which include the multi-wave pattern[50,51], people's mobility between different regions[48,49,52] and the presence of multiple virus variants[5].

Time dependent rates and relation to SIIRV. The eRG approach[29,30] describes the spread of a disease through flow equations (the so called β-functions) and characterises a wave as the flow between fixed points[5,29,49,50]. Concretely, for $\alpha = \phi(I_{\rm c})$, with ϕ a continuous, differentiable and monotonic function, the β-function for a single wave (and a single variant of a disease) can be written as

$$-\beta_\alpha(t) = \frac{d\alpha}{dt} = \frac{d\phi}{dI_{\rm c}}\frac{dI_{\rm c}}{dt} = \lambda_0\,\alpha\left(1-\frac{\alpha}{A_0}\right)^{2d}, \tag{8}$$

with (A_0,λ_0,d) constants. Here, λ_0 is related to the infection rate of the disease, while A_0 is the asymptotic number of individuals who get infected during the wave. For simplicity, we shall consider $d=\frac{1}{2}$ and $\alpha=\phi(I_{\rm c})=I_{\rm c}$ in the following. In this case, the solution of the flow equation (8) is a logistic function

$$I_{\rm c}(t) = \frac{A_0}{1+e^{-\lambda_0(t-t_0)}}, \tag{9}$$

where $t_0\in\mathbb{R}$ is an integration constant that gives the timing of the maximum of infectious individuals during the wave. As demonstrated in the literature[5,29,30,48,49], and shown in more examples in Section S6 of the Supplementary Material, for suitable values of the parameters (A_0,λ_0,t_0), the function (9) describes accurately the time evolution of infected individuals during a single wave of COVID-19 even for populations that differ greatly geographically as well as socio-culturally and under very different circumstances regarding non-pharmaceutical interventions, vaccines and variants of SARS-Cov-2 .

As the eRG only describes the cumulative number of infected individuals $I_{\rm c}$, in order to match the solutions to those of the SIIRV compartmental model introduced in the previous subsection, we need to make a further assumption on how the cumulative number of infected individuals is distributed among removed and infectious individuals. To this end we assume that

$$I(t) = \int_{t-\tau}^{t} dt\,\frac{dI_{\rm c}(t')}{dt'}\,dt' = I_{\rm c}(t) - I_{\rm c}(t-\tau), \tag{10}$$

represents the total number of infectious individuals (either vaccinated or unvaccinated) at time t, where τ is the average amount of time an infectious individual remains infectious. We have verified that this assumption does not play any crucial role in the following analysis, and that it is compatible with the epidemiological data in Germany and Austria (see Supplementary Material for more details). Furthermore, in order to reproduce the cumulative number of infected (9) along with $I(t)=N(I_1+I_2)(t)$ in (10) with the SIIRV model (1) and (2), it is generally required that the infection and recovery rates of the compartmental model are functions of time[30]. We first validated the matching in a simple scenario, with fixed ratio σ_2/σ_1 and in absence of vaccinations (i.e. $\rho=0$ and $V_0=0$). An typical example of time-dependent (σ_1,ε) matching to the eRG solution is shown in Fig. 2. Functions of this form were previously found[30] when matching the eRG approach to a time-dependent SIR model. More precisely, as is showcased by the black interpolating lines in Fig. 2, the time dependence of $(\sigma_1(t),\varepsilon(t))$ can be approximated by logistic functions of the form

$$\sigma_1(t) = A_\sigma\left(1-\frac{1}{1+e^{-\lambda_\sigma(t-t_\sigma)}}\right)+\delta_\sigma, \quad \varepsilon(t) = \frac{A_\varepsilon}{1+e^{-\lambda_\varepsilon(t-t_\varepsilon)}}+\delta_\varepsilon, \tag{11}$$

where $\lambda_\sigma\sim\lambda_\varepsilon\sim\lambda_0$ and $t_\sigma\sim t_\varepsilon\sim t_0$ while $(A_\sigma,\delta_\sigma,A_\varepsilon,\lambda_\varepsilon)$ show a more complicated dependence on (A_0,λ_0,t_0).

Vaccinations. Next we consider a non-vanishing number of (fully) vaccinated individuals at the outbreak of the wave, $V_0\neq 0$, and a non-trivial vaccination rate ρ. We first study the impact of V_0 on the eRG model ($\rho=0$) when it remains below the herd immunity threshold. We find convenient to match the solutions of the SIIRV model to a logistic function in the form

$$I_{\rm c}(t) = \frac{A_0(1-\kappa V_0)}{1+e^{-\lambda_0(t-t_0)}}, \tag{12}$$

where κ is a numerical parameter close in value to $h^{\rm HIT}$. As explained in the Supplementary material, this is still accomplished by a functional dependence of the form (11) for $(\sigma_1(t),\varepsilon(t))$ with a roughly linear dependence of A_σ on V_0.

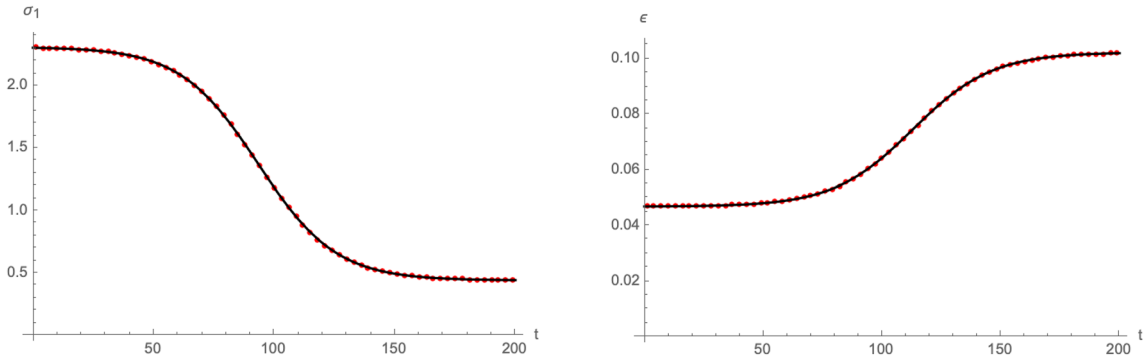

Figure 2. Time dependence of the infection rate σ_1 (left panel) and the removal rate ε (right panel) needed to reproduce and $I_c(t)$ of the form (9) with the compartmental model (1) (red dots). Both plots use $A_0 = 0.025$, $\lambda_0 = 0.06, t_0 = 100, \tau = 14, \rho = 0, \zeta = 0, \sigma_2/\sigma_1 = 1$ and $V_0 = 0$. The interpolating black lines correspond to approximations with logistic functions following (11) with notably $A_\sigma = 1.87, \delta_\sigma = 0.44, A_\varepsilon = 0.055$ and $\delta_\varepsilon = 0.047$.

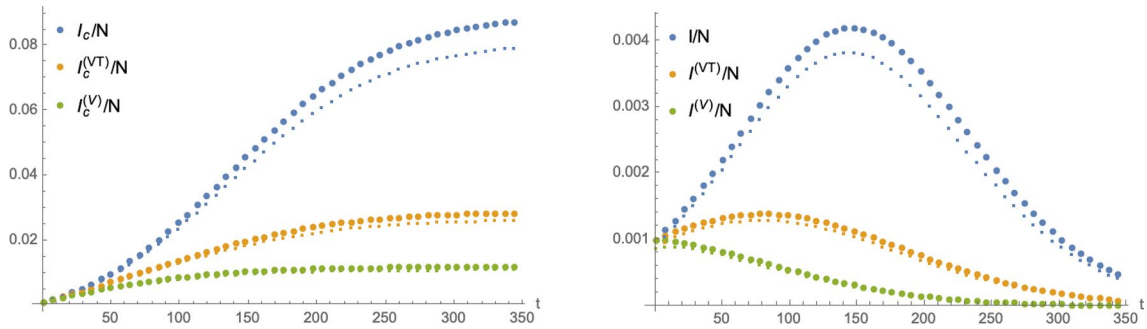

Figure 3. Numerical solutions of the SIIRV model with different variants of a HP: solutions of Eq. (1) are represented by blue points, those of Eq. (4) by orange points and those of (6) by green points. The left panel shows the cumulative number of infected individuals (large points stand for the total numbers, while small points represent only the unvaccinated individuals) and the right panel the infectious individuals as functions of time. Both plots use $\sigma_1 = \sigma_2 = 1.6, \varepsilon = 0.1, \zeta = 0.15, \rho = 0.0005$ and $V_0 = 0.3$.

Finally we turn on the vaccination rate ρ. For the eRG framework, the dependence of I_c on the vaccination rate has been discussed[52], and it has been proposed to promote λ_0 and A_0 to dynamical functions of time that follow the additional first-order differential equations

$$\frac{d\lambda_0}{dt} = -\rho\lambda_0(t=0)\,, \quad \text{and} \quad \frac{dA_0}{dt} = -\rho\,(A_0(t) - I_c(t))^w\,. \tag{13}$$

in supplement to the β-function (8). This implies $\lambda_0(t) = \lambda_0(t=0)[1 - t\,\rho]$, while the second equation in (13) for $w = 1$ derives from the fact that, at any given time t, the reduction of the asymptotic cumulative number of infected individuals can only depend on remaining number of susceptible $A_0(t) - I_c(t)$[52]. As further explained in Section S4 of the Supplementary Material, here we find that a better match with the solutions of the SIIRV model can be obtained with $w \in [0, 1)$.

Health pass models. Having established a correspondence between the eRG approach and the SIIRV model (1) and (2) with non-constant rates, we next assume that the time dependence of (σ_1, ε) remains valid also after implementing either of the two HP models (4) or (6) and the only modification is due to the (constant) parameter p_{VT} and p_V respectively. In this case, numerical solutions indicate that the cumulative number of infected individuals can still be well approximated by a logistic function (9) (see the left panel of Fig. 4), albeit with p-dependent parameters (A_0, λ_0, t_0) as shown in the right panel of Fig. 4.

Ethical approval. The methods employed in this work are in accordance with all the relevant guidelines and regulations.

Results

General results. Numerical solutions of the SIIRV model (1) and (2) as well as the two HP-modifications (4) and (6) are shown in Fig. 3. The right panel of this figure demonstrates the potential of a HP to 'flatten the curve', i.e. to reduce the local maximum of the number of infectious individuals as a function of time, or even

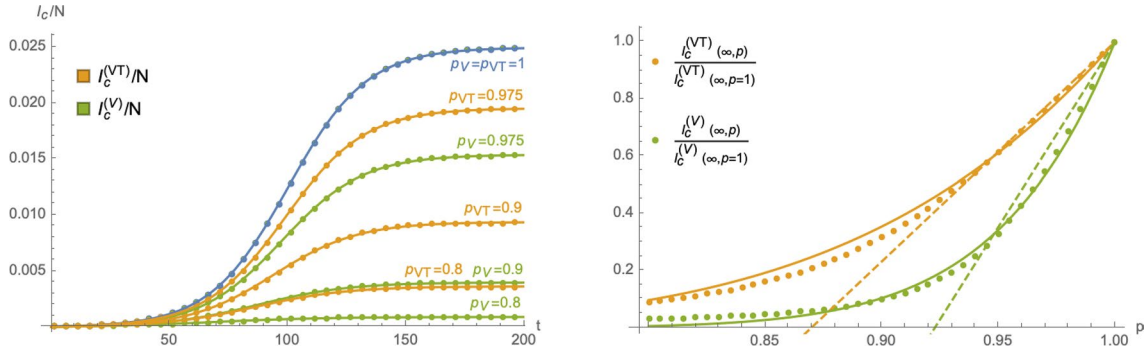

Figure 4. Left panel: cumulative number of infected in the two compartmental HP-models with time dependent parameters (σ_1, ε) as a function of p_{VT} and p_V: orange curves represent the model (4) and green curves the model (6). The blue curve (with $p_{VT} = p_V = 1$) is identical in both models (and corresponds to the case of no HP in (1)). Right panel: comparison of the asymptotic cumulative number of infected individuals as a function of p (and normalised to $p = 1$) for (4) and (6). The dots represent the numerical solutions, while the dashed lines stand for the leading (linear) approximation at $p = 1$ and the solid lines for interpolations with exponential functions of the form (14). The plot uses $\sigma_1 = \sigma_2 = 1.6, \varepsilon = 0.1, \zeta = 0.15, \rho = 0.0005$ and $V_0 = 0.3$ and leads to the interpolation parameters $\theta^{(VT)} = 9.326$ and $\theta^{(V)} = 20.364$.

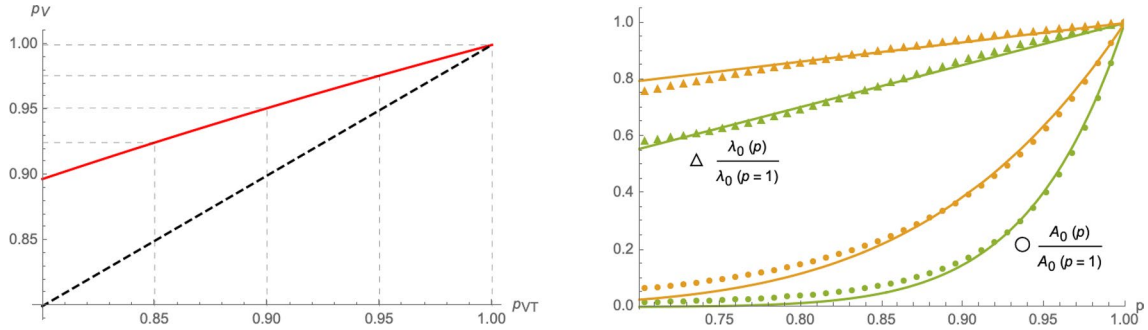

Figure 5. Left panel: using the same numerical parameters as in Fig. 4, the red curve represents the relation between the p-parameters of (4) and (6) that lead to the same asymptotic cumulative number of infected individuals. The dashed black line represents for comparison the relation $p_V = p_{VT}$. Right panel: p-dependence of the parameters (A_0, λ_0) relative to the case $p = 1$ in the eRG approach equivalent to the SIIRV model with time dependent rates: circles represent numerical values of $\frac{A_0(p)}{A_0(p=1)}$ while triangles represent numerical values of $\frac{\lambda_0(p)}{\lambda_0(p=1)}$, with orange symbols computed using the model (4) and green symbols correspond to the model (4). The solid lines represent interpolations of the numerical solutions with an exponential function of the form (16) for $\frac{A_0(p)}{A_0(p=1)}$ and a linear function for $\frac{\lambda_0(p)}{\lambda_0(p=1)}$. The plots use $A_0 = 0.025$, $\lambda_0 = 0.06$ (at $t = 0$), $t_0 = 100, V_0 = 0.3$ and $\zeta = 0.15$.

completely eliminate it. To further study this point, the left panel of Fig. 4 shows the cumulative number of infected individuals for the two compartmental HP-models (4) and (6). The right panel of this figure shows a comparison of their asymptotics (i.e. at the end of the wave) as a function of p (and normalised to $p = 1$). For a certain range of $p < 1$, the numerical solutions can be interpolated by exponential functions of the form

$$I_c^{(VT,T)}(\infty, p) \sim I_c^{(VT,T)}(\infty, p = 1) \exp\left(\theta^{(VT,T)} \frac{p-1}{p}\right), \quad \text{with} \quad \theta^{(VT,T)} \in \mathbb{R}_+, \tag{14}$$

with the two models mainly differing by the constant fitting parameters $\theta^{(VT)}$ and $\theta^{(V)}$. In fact, approximations of this type are already viable within the framework of a SIR model[14] without any vaccination dynamics. More details, including a comparison of (14) with the first and second order of a Taylor series expansion around $p = 1$ can be found in the Supplementary Material. Assuming all remaining parameters to be the same (notably the recovery rate ε), the same efficacy of the HP-models (4) and (6), p_{VT} and p_V respectively, lead to different asymptotic cumulative numbers of infected individuals. We can turn this relation around by determining which values of p_{VT} and p_V (for all other parameters being held fixed), lead to the same number of infected individuals at the end of the epidemic wave. The red line in the left panel of Fig. 5 shows the relation between p_V and p_{VT} that needs to be satisfied in order to obtain the same asymptotic behaviour: for the parameters chosen, $1 - p_{VT}$ in a HP that accepts both test and vaccination certificates needs to be roughly a factor 2 larger than $1 - p_V$ in a HP ,

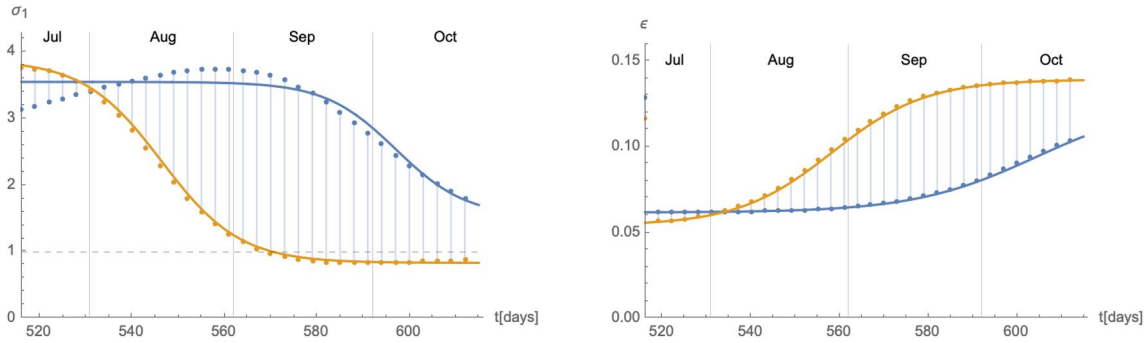

Figure 6. Time dependent parameters σ_1 (left panel) and ε (right panel) for the extremal cases of wave 4. The blue and orange colours are correlated with the curves in the right panel of Fig. F10 in the Supplementary Material.

which only allows vaccinated individuals full access to public life. The relation in the left panel of Fig. 5 can be studied using the approximation (14), which implies equivalent asymptotic numbers of infected individuals for

$$p_{\mathrm{V}} = \frac{p_{\mathrm{V}}\,\theta^{(\mathrm{V})}}{p_{\mathrm{VT}}(\theta^{(\mathrm{V})} - \theta^{(\mathrm{VT})}) + \theta^{(\mathrm{VT})}} = 1 + \frac{\theta^{(\mathrm{VT})}}{\theta^{\mathrm{V}}}\,(p_{\mathrm{VT}} - 1) + \frac{\theta^{(\mathrm{VT})}(\theta^{(\mathrm{VT})} - \theta^{(\mathrm{V})})}{(\theta^{(\mathrm{V})})^2}\,(p_{\mathrm{VT}} - 1)^2 + \mathcal{O}\,((p_{\mathrm{VT}} - 1)^3)\,. \tag{15}$$

The linear approximation around $p_{\mathrm{VT}} = 1$ with the coefficient $\frac{\theta^{(\mathrm{VT})}}{\theta^{\mathrm{V}}} \sim 0.458$ indeed very well agrees with the left panel of Fig. 5. We stress, however, that this comparison assumes that all remaining parameters of the system remain the same for both models. In particular, we assumed the same removal rate ε in both cases, which (among other things) depends on the efficiency of the contact-tracing, i.e. identifying and quarantining infected individuals and therefore also crucially depends on the number of tests that are being performed per time unit. Since a V-HP-model offers less incentive for individuals to get tested (unless they present clear symptoms), they likely also entail a lower test rate, leading ultimately to a smaller value of ε. A numerical equivalence taking into account a possible change in ε is discussed in Section S5 of the Supplementary Material.

From the perspective of the eRG, which is equivalent to the SIIRV models (4) and (6) with time dependent infection and removal rates of the form (11), relation (14) implies that a HP can be implemented by allowing for a p-dependence of A_0 and λ_0 in the β-function (8), concretely

$$A_0(p) \sim A_0(p=1)\exp\left(\theta\,\frac{p-1}{p}\right), \qquad \text{with} \qquad \theta \in \mathbb{R}_+. \tag{16}$$

The constant θ implicitly depends on the remaining parameters of the problem (notably the vaccination dynamics and $A_0(p=1)$). The p dependence of λ_0 for small $1-p$ can be approximated to be linear, as is shown in the right panel of Fig. 5.

Examples. We next apply the theoretical results developed above to the epidemiological situation of Germany and Austria in the late summer/early fall of 2021. Further examples of France, Italy and Denmark are discussed in Section S6 of the Supplementary Material.

Germany. The epidemiological situation in Germany since the beginning of the COVID-19 pandemic and the summer of 2021 is shown in Section S6.2 of the Supplementary Material. The available data for an impending wave from 07/July/2021 to 17/August/2021 can be fitted with a logistic function of the form

$$I_{\mathrm{c}}^{\mathrm{wave}}(t) = I_{\mathrm{c},0} + \frac{A_0}{1 + e^{-\lambda_0(t-t_0)}}\,, \tag{17}$$

which however shows a large uncertainty when extrapolated until the middle of September. We therefore consider as two extremal cases logistic functions parametrised by (for more information see the Supplementary Material)

$$\begin{aligned} A_0^+ &= 2.5\cdot 10^6\,, \quad \lambda_0^+ = 0.072\,, \quad t_0^+ = 594.5\,, \quad \delta_0^+ = 3.74\cdot 10^6\,, \\ A_0^- &= 174533\,, \quad \lambda_0^- = 0.094\,, \quad t_0^- = 548.3\,, \quad \delta_0^- = 3.74\cdot 10^6\,. \end{aligned} \tag{18}$$

Based on these values, we can develop a time-dependent SIIRV model, with time dependent parameters (σ_1, ε), which are shown in Fig. 6. These curves follow the general form of Eq. (11) with the parameters

	$A^+_{\sigma,\varepsilon}$	$A^-_{\sigma,\varepsilon}$	$\lambda^+_{\sigma,\varepsilon}$	$\lambda^-_{\sigma,\varepsilon}$	$t^+_{\sigma,\varepsilon}$	$t^-_{\sigma,\varepsilon}$	$\delta^+_{\sigma,\varepsilon}$	$\delta^-_{\sigma,\varepsilon}$
σ_1	2.024	3.047	0.131	0.119	81.1	30.4	1.529	0.838
ε	0.065	0.085	0.072	0.094	88.5	42.3	0.062	0.054

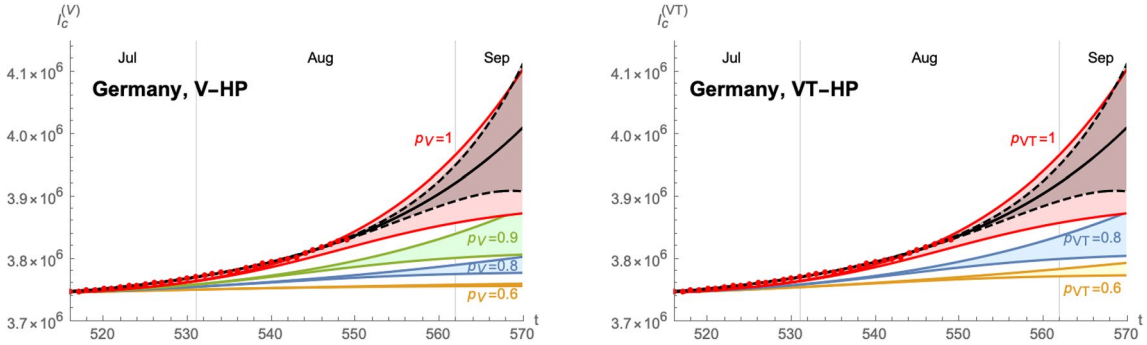

Figure 7. Time evolution of the cumulative number of infected individuals for different values of the efficacy of a V-HP (right panel) or a VT-HP (right panel). We assume that the model has been introduced on 07/07/2021. Both cases use $\zeta = 0.15$ (based on an average of the efficacy of each vaccine weighted by the distribution among the population), $\rho = 0.008$ and $\sigma_2/\sigma_1 = 1$.

Finally, implementing the Green pass model based on these extremal cases is shown in Fig. 7. Starting from the band of cumulative number of infected individuals (for $p = 1$), we obtain a similar band for each $p < 1$. The plots for a VT-HP and V-HP respectively are shown for $\sigma_2/\sigma_1 = 1$ in Fig. 7, assuming that the HP has been introduced on 07/July/2021. Figure 8 shows the same analysis assuming that the HP had been introduced on 01/August/2021.The plots in Fig. 7 suggest that a new wave in Germany could be stopped by reducing the contacts among non-vaccinated individuals by roughly 20–40%. Finally, we have compared the efficacy of the VT-HP and V-HP in the case of Germany in Fig. 9: the left panel shows the (normalised) cumulative number of infected individuals at $t_f = 15/September/2021$, along with an approximation of the form (16). Notice, rather than the asymptotic number of infected individuals at the end of the wave, we have chosen a date roughly a months after the last available data for the comparison. The right panel shows which values of p_V and p_{VT} lead to the same cumulative number of infected individuals at t_f: the red band corresponds to the uncertainty related to the two extremal cases we have developed to extrapolate the data. In fact, the extrema of this band arise when comparing the most optimistic extrapolation for the V-HP with the worst case approximation of VT-HP (and vice versa). The blue line corresponds to a comparison of equivalent extrapolations and suggests roughly

$$2(1 - p_V) \sim 1 - p_{VT}\,. \tag{19}$$

This means, assuming that all other parameters remain roughly the same, the reduction in the contacts in the VT-HP needs to be roughly twice as large as in the V-HP-model to achieve the same cumulative number of infected.

Austria. The epidemiological situation in Austria since the beginning of the COVID-19 pandemic and the summer of 2021 is shown in Section S6.3 of the Supplementary Material. As in Germany, the available data from 01/July/2021 to 17/August/2021 show a great uncertainty when extrapolated until middle of September. We therefore again fit two extremal logistic functions of the form (17), with the exact numerical data given in Section S6.3 of the Supplementary Material. These data suggest the onset of a new wave, just as in the case of Germany. However, unlike Germany, a VT-HP (3-G-rule: 'geimpft, getestet, genesen') was enforced on 01/July/2021, with earlier measures dating as far back as 19/May/2021 (the rule was slightly modified on 22/07 and 15/08 specifying stricter rules to discotheques and nightclubs and imposing restrictions to only partially vaccinated individuals respectively, see the Supplementary Material for further details) allowing individuals full access to the public life only with a certificate of either being (fully) vaccinated, having recovered from a previous infection or having tested negative for SARS-Cov-2 . Therefore, in order to derive time-dependent parameters $(\sigma_1(t), \varepsilon(t))$ for the above mentioned extremal cases, we need to take the presence of the V-HP into account. Since the exact efficacy of the HP are difficult to quantify, we have used $p = 0.8$ and $p = 0.9$ as reference values to fit the data. The corresponding time-dependent functions $(\sigma_1(t), \varepsilon(t))$ for wave 4 are shown in Fig. 10. As is evident, the main difference lies in the function σ_1, while the curve for ε is relatively unchanged. Indeed, as remarked before, mathematically the parameter p_{VT} can be absorbed in the γ_1. Since we assumed for the latter anyway a certain range, the main effect of p_{VT} can also be absorbed in the quotient σ_2/σ_1, i.e. the reduction in the rate at which vaccinated infectious individuals infect others. We next apply these time-dependent (σ_1, ε) parameters to the stronger V-HP model (6). The results are shown in Fig. 11. The results again support an equivalence of the type (19) between the parameters p_V of the V-HP and p_{VT} of the VT-HP model.

Conclusions

In this paper we have analysed the impact of Health Passes on the epidemiological dynamics of infectious diseases. These HPs correspond to measures that restrict the access of individuals with a higher risk of being infectious to public life. Concretely, we have distinguished two different classes that grant access to individuals with a vaccination certificate or a recent negative test (VT-HP) and only to vaccinated individuals (V-HP).

We have first discussed these HPs in the context of a simple compartmental SIIRV model (1) and have generalised them in the context of the eRG framework, which is better suited for describing the dynamics over a

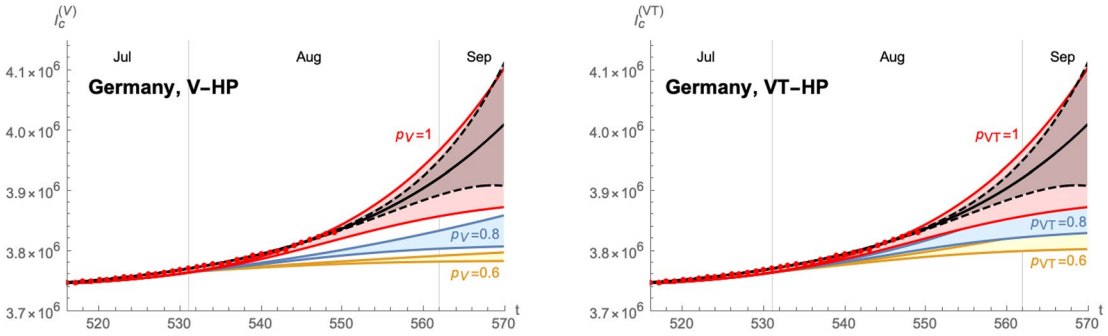

Figure 8. Time evolution of the cumulative number of infected individuals for different values of the efficacy of a V-HP (right panel) or a VT-HP (right panel). We assume that the model has been introduced on 01/08/2021. Both cases use $\zeta = 0.15$ (based on an average of the efficacy of each vaccine weighted by the distribution among the population), $\rho = 0.008$ and $\sigma_2/\sigma_1 = 1$.

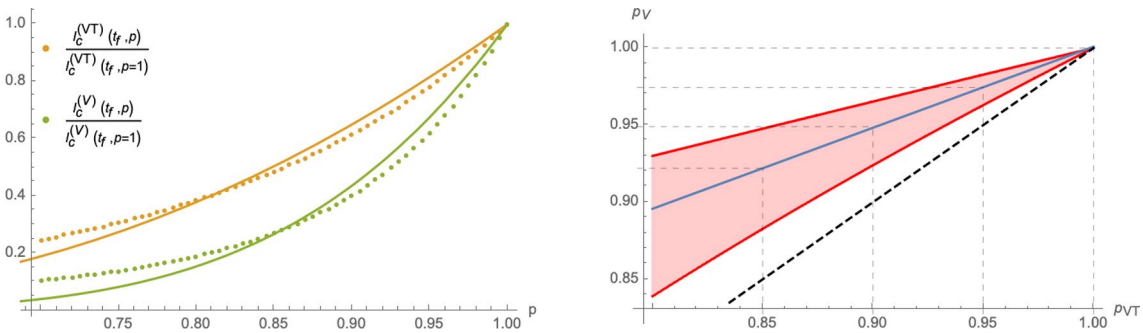

Figure 9. Comparison of the V-HP model (6) and the VT-HP model (4): the left panel shows the cumulative number of infected individuals at $t_f = 15/09/2021$ as a function of p (normalised to the value of $p = 1$). The orange curve corresponds to the model (6) and the green curve to the one in (4). The right panel shows the equivalence for the parameters p_{VT} and p_{V} of these two models, taking into account the incertitude inherent in the approximations: the red band indicates equivalent values of these parameters that lead to the same value of $I_c(t_f)$ with the blue line corresponding to equivalence obtained comparing equivalent extrapolations of the data in each case.

longer period of time, in particular an entire epidemiological wave. Analysing in particular the dependence of the asymptotic cumulative number of infected individuals (which is a crucial parameter in the description of the eRG), we have found the approximative exponential dependence (16) on the parameter describing the efficacy of the HP . Furthermore, comparing the efficacy of a VT-HP-model to a V-HP model reduces to comparing the corresponding θ-parameters appearing in this approximation.

We have furthermore validated our models by discussing the diffusion of COVID-19 in several European countries. We have analysed in detail Germany (who, to this date, has not implemented any HP) and Austria (who currently has implemented a VT-HP and considers the partial introduction of a V-HP) and have presented a briefer analysis for France, Denmark and Italy. In all cases we have established that a V-HP is much more efficient in reducing the number of infected. Our model in fact allows for a quantitative comparison, leading to the relation (19): if all remaining parameters remain the same, the efficacy of a VT-HP needs to roughly be twice as high to produce the same reduction of infections as a V-HP . Furthermore in most cases, an efficiency of a V-HP of roughly 20-40% is strong enough to completely suppress a potential fourth wave.

We have undertaken preliminary studies that also include a potential reduction in the number of tests (related to a reduction in the removal rate due to a reduced capacity of identifying and isolating infected individuals). It would be important to further extend these studies, in particular to establish a quantitative relation between these two rates.

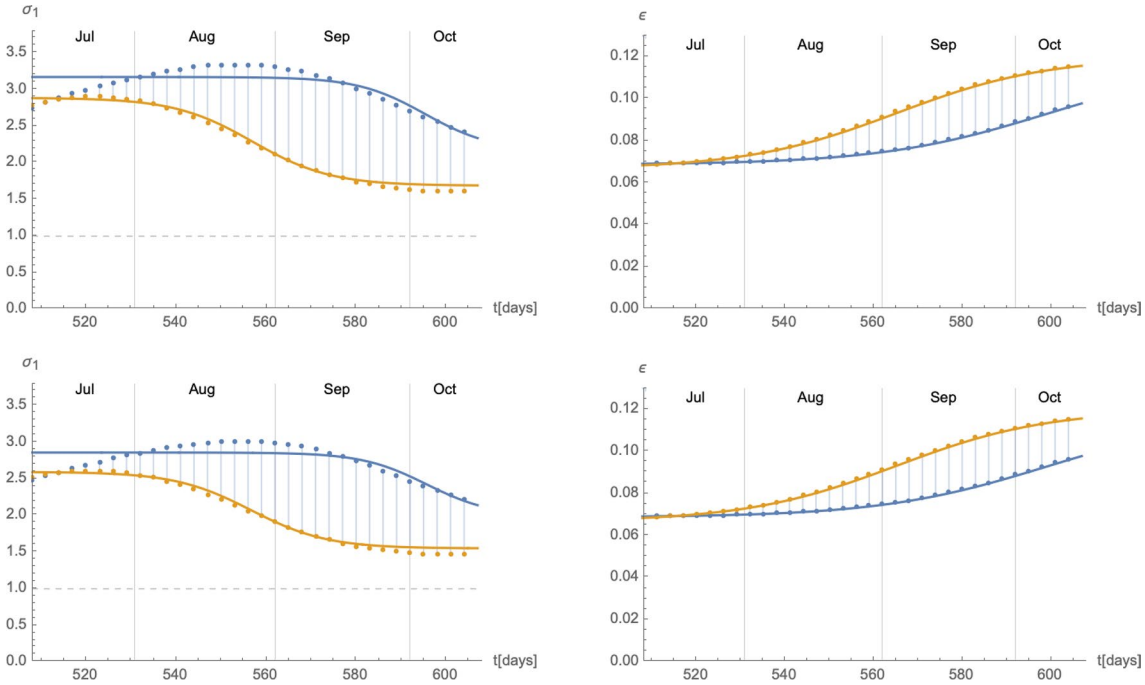

Figure 10. Time dependent parameters σ_1 (left panel) and ε (right panel) for the extremal cases of wave 4. The blue and orange colours are correlated with the curves in the right panel of Figure F10. The panels of the top row use $p = 0.8$, while the panels in the bottom row use $p = 0.9$ in order to fit the data.

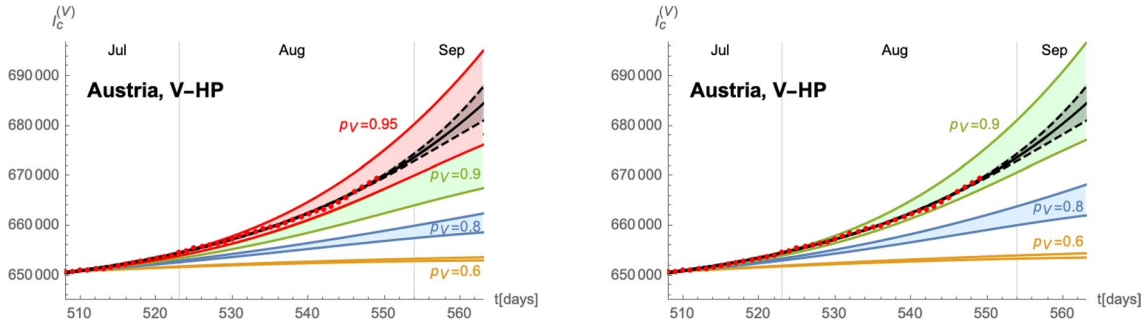

Figure 11. Predicted time evolution of the cumulative number of infected individuals for different values of the efficacy p_V of the V-HP model. The left panel assumes $p_{VT} = 0.9$ for the VT-HP currently in place in Austria and the right panel $p_{VT} = 0.8$. Both plots assume furthermore $\sigma_2/\sigma_1 = 1$ and $\rho = 0.0085$.

Data availability

The epidemiological data are extracted from the open-source repository on Worldometer. Data about the vaccination rates and progression have been downloaded from the Robert Koch Institute for Germany[55], and from the Austrian Ministry webpage for Austria[56].

Received: 29 October 2021; Accepted: 30 March 2022
Published online: 28 April 2022

References

1. Korber, B. *et al.* Tracking changes in SARS-CoV-2 spike: Evidence that D614G increases infectivity of the COVID-19 virus. *Cell* **182**, 812-827.e19. https://doi.org/10.1016/j.cell.2020.06.043 (2020).
2. Mahase, E. Covid-19: What have we learnt about the new variant in the UK?. *BMJ* https://doi.org/10.1136/bmj.m4944 *(2020).*
3. Rambaud, A. *et al.* Preliminary genomic characterisation of an emergent SARS-CoV-2 lineage in the UK defined by a novel set of spike mutations. *COVID-19 Genomics Consortium UK (CoG-UK) Report* (2020).
4. Volz, E. *et al.* Transmission of SARS-CoV-2 lineage b.1.1.7 in England: Insights from linking epidemiological and genetic data. *medRxiv*. https://doi.org/10.1101/2020.12.30.20249034 (2021). https://www.medrxiv.org/content/early/2021/01/04/2020.12.30.20249034.1.full.pdf.

5. Cacciapaglia, G. *et al.* Epidemiological theory of virus variants. *Phys. A* **596**, 127071. https://doi.org/10.1016/j.physa.2022.127071 (2022). arXiv:2106.14982.
6. de Hoffer, A. *et al.* Variant-driven multi-wave pattern of COVID-19 via machine learning clustering of spike protein mutations. *medRxiv*. https://doi.org/10.1101/2021.07.22.21260952 (2021). https://www.medrxiv.org/content/early/2021/07/24/2021.07.22.21260952.full.pdf.
7. Chang, S. *et al.* Mobility network models of COVID-19 explain inequities and inform reopening. *Nature* **589**, 82–87. https://doi.org/10.1038/s41586-020-2923-3 (2021).
8. Doi, M. Second quantization representation for classical many-particle system. *J. Phys. A Math. Gen.* **9**, 1465 (1976).
9. Doi, M. Stochastic theory of diffusion-controlled reaction. *J. Phys. A Math. Gen.* **9**, 1479. https://doi.org/10.1016/S0378-4371(03)00458-8 (1976).
10. Peliti, L. Path integral approach to birth-death processes on a lattice. *J. Phys. France (Paris)* **46**, 1469–1483. https://doi.org/10.1051/jphys:019850046090146900 (1985).
11. Domb, C. Fluctuation phenomena and stochastic processes. *Nature* **184**, 509–12. https://doi.org/10.1038/184509a0 (1959).
12. Cardy, J. L. & Grassberger, P. Epidemic models and percolation. *J. Phys. A Math. Gen.* **18**, L267–L271. https://doi.org/10.1088/0305-4470/18/6/001 (1985).
13. Grassberger, P. On the critical behavior of the general epidemic process and dynamical percolation. *Math. Biosci.* **63**, 157–172. https://doi.org/10.1016/0025-5564(82)90036-0 (1983).
14. Kermack, W. O., McKendrick, A. & Walker, G. T. A contribution to the mathematical theory of epidemics. *Proc. R. Soc. A* **115**, 700–721. https://doi.org/10.1098/rspa.1927.0118 (1927).
15. Hethcote, H. W. Qualitative analyses of communicable disease models. *Math. Biosci.* **28**, 335–356. https://doi.org/10.1016/0025-5564(76)90132-2 (1976).
16. Hethcote, H. W. The mathematics of infectious diseases. *SIAM Rev.*https://doi.org/10.1137/S0036144500371907 *(2000).*
17. Stone, L., Shulgin, B. & Agur, Z. Theoretical examination of the pulse vaccination policy in the SIR epidemic model. *Math. Comput. Modell.* **31**, 207–215 (2000).
18. Shulgin, B., Stone, L. & Agur, Z. Pulse vaccination strategy in the SIR epidemic model. *Bull. Math. Biol.* **60**, 1123–1148. https://doi.org/10.1016/S0092-8240(98)90005-2 (1998).
19. Gao, S., Chen, L., Nieto, J. J. & Torres, A. Analysis of a delayed epidemic model with pulse vaccination and saturation incidence. *Vaccine* **24**, 6037–6045. https://doi.org/10.1016/j.vaccine.2006.05.018 (2006).
20. Gao, S., Chen, L. & Teng, Z. Pulse vaccination of an SEIR epidemic model with time delay. *Nonlinear Anal. Real World Appl.* **9**, 599–607. https://doi.org/10.1016/j.nonrwa.2006.12.004 (2008).
21. Breiman, L. Statistical modeling: The two cultures (with comments and a rejoinder by the author). *Stat. Sci.* **16**, 199–231. https://doi.org/10.1214/ss/1009213726 (2001).
22. Flaxman, A. & Vos, T. Machine learning in population health: Opportunities and threats. *PLoS Med.* **15**, e1002702. https://doi.org/10.1371/journal.pmed.1002702 (2018).
23. Wiemken, T. *et al.* Using cluster analysis of cytokines to identify patterns of inflammation in hospitalized patients with community-acquired pneumonia: A pilot study. *J. Respir. Infect.*https://doi.org/10.18297/jri/vol1/iss1/1/ *(2017).*
24. Motsinger-Reif, A., Dudek, S., Hahn, L. & Ritchie, M. Comparison of approaches for machine-learning optimization of neural networks for detecting gene-gene interactions in genetic epidemiology. *Genet. Epidemiol.* **32**, 325–40. https://doi.org/10.1002/gepi.20307 (2008).
25. Ramasubramanian, A. *et al.* High-throughput discovery of targeted, minimally complex peptide surfaces for human pluripotent stem cell culture. *ACS Biomater. Sci. Eng.* **7**, 1344–1360. https://doi.org/10.1021/acsbiomaterials.0c01462 (2021).
26. Wang, Z., Andrews, M. A., Wu, Z.-X., Wang, L. & Bauch, C. T. Coupled disease-behavior dynamics on complex networks: A review. *Phys. Life Rev.* **15**, 1–29. https://doi.org/10.1016/j.plrev.2015.07.006 (2015).
27. Perc, M. *et al.* Statistical physics of human cooperation. *Phys. Rep.* **687**, 1–51. https://doi.org/10.1016/j.physrep.2017.05.004 (2017).
28. Zhan, X.-X. *et al.* Coupling dynamics of epidemic spreading and information diffusion on complex networks. *Appl. Math. Comput.* **332**, 437–448. https://doi.org/10.1016/j.amc.2018.03.050 (2018).
29. Della Morte, M., Orlando, D. & Sannino, F. Renormalization group approach to pandemics: The COVID-19 case. *Front. Phys.* **8**, 144. https://doi.org/10.3389/fphy.2020.00144 (2020).
30. Della Morte, M. & Sannino, F. Renormalisation group approach to pandemics as a time-dependent SIR model. *Front. Phys.* **8**, 583. https://doi.org/10.3389/fphy.2020.591876 (2021).
31. Silal, S. P., Little, F., Barnes, K. I. & While, L. J. Sensitivity to model structure: A comparison of compartmental models in epidemiology. *Health Syst.* **5**, 178–191. https://doi.org/10.1057/hs.2015.2 (2016).
32. Aba Oud, M. A. *et al.* A fractional order mathematical model for COVID-19 dynamics with quarantine, isolation, and environmental viral load. *Adv. Differ. Equ.* **2021**, 106. https://doi.org/10.1186/s13662-021-03265-4 (2021).
33. Asamoah, J. K. K. *et al.* Global stability and cost-effectiveness analysis of COVID-19 considering the impact of the environment: Using data from Ghana. *Chaos Solitons Fractals* **140**, 110103. https://doi.org/10.1016/j.chaos.2020.110103 (2020).
34. Khan, M. A. & Atangana, A. Modeling the dynamics of novel coronavirus (2019-ncov) with fractional derivative. New trends of numerical and analytical methods for engineering problems.. *Alex. Eng. J.* **59**, 2379–2389. https://doi.org/10.1016/j.aej.2020.02.033 (2020).
35. Asamoah, J. K. K. *et al.* Sensitivity assessment and optimal economic evaluation of a new COVID-19 compartmental epidemic model with control interventions. *Chaos Solitons Fractals* **146**, 110885. https://doi.org/10.1016/j.chaos.2021.110885 (2021).
36. Asamoah, J. K. K. *et al.* Optimal control and comprehensive cost-effectiveness analysis for COVID-19. *Results Phys.* **33**, 105177. https://doi.org/10.1016/j.rinp.2022.105177 (2022).
37. Brauner, J. M. *et al.* Inferring the effectiveness of government interventions against COVID-19. *Science* **371**(6531), eabd9338. https://doi.org/10.1126/science.abd9338 (2021).
38. Sharma, M. *et al.* Understanding the effectiveness of government interventions against the resurgence of COVID-19 in Europe. *Nat. Commun.* **12**(1), 5820. https://doi.org/10.1038/s41467-021-26013-4 (2021).
39. Li, Y. *et al.* The temporal association of introducing and lifting non-pharmaceutical interventions with the time-varying reproduction number (R) of SARS-CoV-2: A modelling study across 131 countries. *Lancet Infect. Dis.* **21**(2), 193–202. https://doi.org/10.1016/S1473-3099(20)30785-4 (2021).
40. Liu, Y., Morgenstern, C., Kelly, J., Lowe, R. & Jit, M. The impact of non-pharmaceutical interventions on SARS-CoV-2 transmission across 130 countries and territories. *BMC Med.* **19**(1), 40. https://doi.org/10.1186/s12916-020-01872-8 (2021).
41. Cacciapaglia, G. *et al.* The field theoretical ABC of epidemic dynamics. arXiv:2101.11399 (2021).
42. Giordano, G. *et al.* Modelling the COVID-19 epidemic and implementation of population-wide interventions in Italy. *Nat. Med.* **26**, 855–860. https://doi.org/10.1038/s41591-020-0883-7 (2020).
43. Dashtbali, M. & Mirzaie, M. A compartmental model that predicts the effect of social distancing and vaccination on controlling COVID-19. *Sci. Rep.* **11**, 8191. https://doi.org/10.1038/s41598-021-86873-0 (2021).
44. Balabdaoui, F. & Mohr, D. Age-stratified discrete compartment model of the COVID-19 epidemic with application to Switzerland. *Sci. Rep.* **10**, 21306. https://doi.org/10.1038/s41598-020-77420-4 (2020).
45. Wilson, K. G. Renormalization group and critical phenomena. 1. Renormalization group and the Kadanoff scaling picture. *Phys. Rev. B* **4**, 3174–3183. https://doi.org/10.1103/PhysRevB.4.3174 (1971).

46. Wilson, K. G. Renormalization group and critical phenomena. 2. Phase space cell analysis of critical behavior. *Phys. Rev. B* **4**, 3184–3205. https://doi.org/10.1103/PhysRevB.4.3184 (1971).
47. Banks, T. & Zaks, A. On the phase structure of vector-like gauge theories with massless fermions. *Nucl. Phys. B* **196**, 189–204. https://doi.org/10.1016/0550-3213(82)90035-9 (1982).
48. Cacciapaglia, G. & Sannino, F. Interplay of social distancing and border restrictions for pandemics (COVID-19) via the epidemic Renormalisation Group framework. *Sci. Rep.* **10**, 15828. https://doi.org/10.1038/s41598-020-72175-4 (2020). arXiv:2005.04956.
49. Cacciapaglia, G., Cot, C. & Sannino, F. Second wave COVID-19 pandemics in Europe: A temporal playbook. *Sci. Rep.* **10**, 15514. https://doi.org/10.1038/s41598-020-72611-5 (2020). arXiv:2007.13100.
50. Cacciapaglia, G. & Sannino, F. Evidence for complex fixed points in pandemic data. *Front. Appl. Math. Stat.* **7**, 659580. https://doi.org/10.3389/fams.2021.659580 (2021). arXiv:2009.08861.
51. Cacciapaglia, G., Cot, C. & Sannino, F. Multiwave pandemic dynamics explained: How to tame the next wave of infectious diseases. *Sci. Rep.* **11**, 6638. https://doi.org/10.1038/s41598-021-85875-2 (2021). arXiv:2011.12846.
52. Cacciapaglia, G., Cot, C., Islind, A. S., Óskarsdóttir, M. & Sannino, F. Impact of US vaccination strategy on COVID-19 wave dynamics. *Sci. Rep.* **11**(1), 1–11 (2021) arXiv:2012.12004.
53. Cacciapaglia, G., Cot, C. & Sannino, F. Mining Google and Apple mobility data: Temporal anatomy for COVID-19 social distancing. *Sci. Rep.* **11**, 4150. https://doi.org/10.1038/s41598-021-83441-4 (2021). arXiv:2008.02117.
54. Lopez Bernal, J. *et al.* Effectiveness of COVID-19 vaccines against the b.1.617.2 (Delta) variant. *N. Engl. J. Med.* **385**, 585–594. https://doi.org/10.1056/NEJMoa2108891 (2021).
55. Koch-Institut, R. Robert koch-institut. https://www.rki.de/EN/Home (2021).
56. Bundesministerium Soziales, P. u. K., Gesundheit. Coronavirus-aktuelle massnahmen. https://www.sozialministerium.at/Informationen-zum-Coronavirus/ (2021).

Author contributions
All authors contributed to the original ideas behind the manuscript.

Competing interests
The authors declare no competing interests.

Additional information
Supplementary Information The online version contains supplementary material available at https://doi.org/10.1038/s41598-022-10663-5.

Correspondence and requests for materials should be addressed to G.C.

Reprints and permissions information is available at www.nature.com/reprints.

Publisher's note Springer Nature remains neutral with regard to jurisdictional claims in published maps and institutional affiliations.